between end-diastolic volume and filling pressure. This is indeed reasonable, because the pressure-volume relation of the diastolic ventricle is known to be exponential; therefore, the volume-pressure relation should be the inverse of exponential, i.e., logarithmic (12).

Mechanical parameters such as ventricular systolic and diastolic elastance, heart rate, ventricular interdependence, and arterial resistance have been shown to affect CO (22, 24). To clarify therapeutic targets in the management of cardiac patients, it is crucial to relate those mechanical parameters to the CO curve, as we have done with the venous return surface. Modeling the CO curve on the basis of those parameters is clearly required in future studies.

Analysis of the Circulatory Equilibrium

The venous return surface, combined with the integrated CO curve in the three-dimensional diagram, enables us to make intuitive and in-depth analyses of the contribution of the individual system components to hemodynamics. Figure 9 illustrates the effect of left heart failure on circulatory equilibrium. Integrated CO curves, which were experimentally obtained from a dog under normal and left heart failure conditions, are superimposed on the standard venous return surface in Fig. 9*A*. Under the normal condition, the integrated CO curve intersects the surface at a CO of 115 ml·min^{-1}·kg^{-1}, with a P_{RA} of 2.5 mmHg and a P_{LA} of 4.1 mmHg. In contrast, left heart failure lessens the slope of the CO curve and diverts it toward the axis of P_{LA}. At the intersection of the standard surface and the CO curve under left heart failure, although the CO decreased (85 ml·min^{-1}·kg^{-1}), the increase in P_{LA} (9.3 mmHg) was modest. When the stressed blood volume is increased to simulate the baroreflex response (+8 ml/kg), the surface shifts upward (Fig. 9*B*). The intersection reached a new equilibrium point, where P_{LA} increased drastically (15.9 mmHg) with a slight increase in P_{RA} and a partial recovery of CO. Although this analysis is hypothetical, the graphical analysis represents the typical hemodynamics of left heart failure (2, 4, 10, 23, 35). Notwithstanding its simplicity, the framework for the venous return surface provides a very powerful tool for analysis of complicated hemodynamics in the clinical setting.

Comparison with Previous Studies of Cardiovascular Modeling

Many studies have modeled hemodynamics of the cardiovascular system (3–5, 20, 31, 33). The parallel circuit model of Caldini et al. (5) seems to be more appropriate than our serial model for an anatomically oriented analysis of hemodynamics within a single circulation, i.e., the analysis of blood redistribution between the splanchnic and nonsplanchnic circuits. Levy (20) simplified blood distribution between the arterial and venous compartments with a lumped serial model. Although these models could analyze hemodynamics within a single circulation, they were not intended to deal with blood redistribution between the systemic and the pulmonary circulation. In contrast, the two-compartment model of Guyton et al. (15) and the multiple-circuit model proposed by Sylvester et al. (31) can address this issue. These studies, however, went no further than a theoretical analysis and remain insufficient for clinical application. The two-compartment model of Guyton et al. is complicated. It fails to express venous return curves parametrically; consequently, neither the stressed blood volume nor the curve shifts in response to changes in stressed blood volume can be estimated (15). Sylvester et al. (31) integrated systemic and pulmonary venous return curves into a single curve and expressed it parametrically. However, extensive experimental validations of the model are needed. In addition, because the pressure axis of their integrated venous return curve was the weighted average of P_{RA} and P_{LA}, we were unable to uniquely determine their individual values from the equilibrium point in their diagram.

There have been serious debates among cardiovascular physiologists regarding cause-effect relations between CO/venous return and atrial pressure, i.e., which variable determines the others? Brengelmann (3), Levy (20), and Tyberg (33) argued that as CO increases, the venous reservoir is depleted (i.e., blood is translocated from the veins to the arteries), and, therefore, venous pressure (i.e., atrial pressure) decreases. In the heart, atrial pressure determines CO according to the Frank-Starling mechanism. In contrast, in response to the work of Levy, Guyton (14) commented that he considered CO and atrial pressures to be the effects, or dependent variables. Blood volume and the mechanical properties of the heart and vasculature, such as heart rate, ventricular contractility,

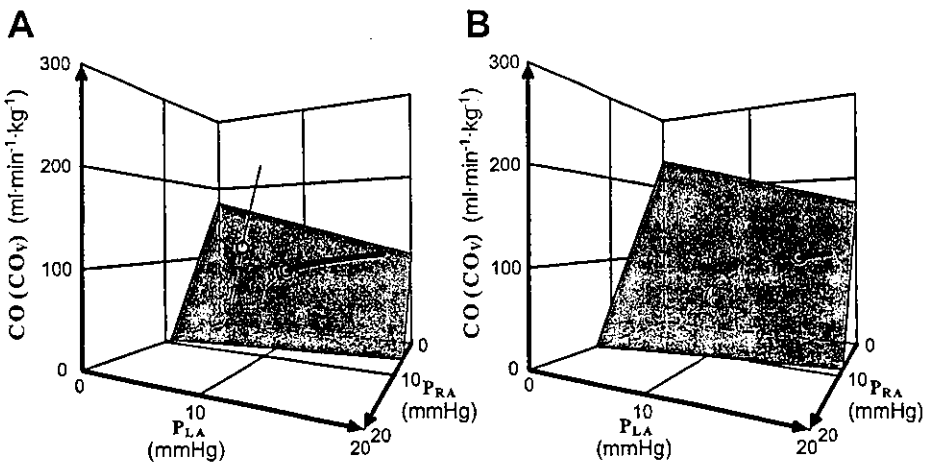

Fig. 9. *A*: integrated CO curves under normal cardiac conditions (thin solid line) and left heart failure condition (thick solid line) superimposed with the standard venous return surface with control stressed blood volume. ○, Intersection of curves and standard venous return surface. Compared with normal hemodynamics (P_{RA} = 2.5 mmHg, P_{LA} = 4.1 mmHg, CO = 115 ml·min^{-1}·kg^{-1}), CO decreased and both P_{LA} and P_{RA} increased under left heart failure (P_{RA} = 3.1 mmHg, P_{LA} = 9.3 mmHg, and CO = 85 ml·min^{-1}·kg^{-1}). *B*: integrated CO curve under left heart failure condition (thick solid line) superimposed with the standard venous return surface with increased stressed blood volume (8 ml/kg). At the new equilibrium point, P_{LA} (15.9 mmHg) drastically increased with a slight increase in P_{RA} (4.0 mmHg) and partial recovery of CO (106 ml·min^{-1}·kg^{-1}).

and vascular resistance, are the cause. The CO curve or venous return curve discloses those properties through the relation between the flow and atrial pressures. As we demonstrated in *Eq. 1*, under a given stressed volume, venous return/CO and atrial pressure have a linear relation. In other words, once venous return is determined, atrial pressure is automatically determined and vice versa. Therefore, our framework is consistent with Guyton's comment on the work of Levy. As far as the prediction of hemodynamics is concerned, however, the difference between their interpretations and ours does not impact the result of this study, because we are able to obtain the same equilibrium point with either interpretation (14, 20).

Application of This Framework

Accurate predictions of CO and filling pressures after therapeutic interventions are vital in the management of heart failure, as suggested by the classification of Forrester (10) and other previous studies (11, 21). Although the Swan-Ganz catheter allows us to estimate CO and filling pressures, such devices do not allow us to estimate the venous return curve or mean circulatory filling pressure (6). In contrast, because the parameter values of the venous return surface were invariable among animals, it is conceivable that the same standard values obtained from this investigation might be used for patients. If this is the case, for given values of CO, P_{LA}, and P_{RA}, all of which can be easily obtained by Swan-Ganz catheters, we can uniquely define the venous return surface and estimate stressed blood volume of patients without the need to perform total heart bypass (6). The clinical usefulness of knowing the venous return surface would be markedly increased if the integrated CO curve could be estimated. This would enable accurate prediction of the CO, P_{RA}, and P_{LA} in response to various therapeutic interventions, which induce changes in loading condition, or changes in the pumping ability of the heart, i.e., changes in CO curves. These should help optimize hemodynamic management and improve patient prognosis (10, 21).

Limitations

In this investigation, we isolated baroreceptors and fixed the autonomic tone. This was necessary, because the baroreflex alters the CO curve and venous return surface through its effects on stressed blood volume, vascular resistance, heart rate, and cardiac contractility (9, 24, 27). How changes in autonomic tone under the closed-loop condition affect the CO curve and venous return surface remains to be investigated.

We assumed that there is no fluid shift between the intravascular and extravascular space and that the volume perturbations exclusively changed the stressed blood volume. We assumed that the changes of cardiac volume and volume shifts between the heart and vasculatures are rather small. However, this may not be the case if the ventricles are extremely compliant, as in those with extensive remodeling (32). In such cases, the volume shifts between the heart and the vasculatures become significant. Further studies are required to clarify these relations to facilitate the future clinical application of this framework.

All the experiments of this study were conducted in anesthetized, open-chest dogs. Anesthesia and surgical trauma affect the cardiovascular system significantly (34). Whether this equilibrium framework can be applied to conscious, closed-chest animals (including humans) remains to be seen. We used two pumps for total heart bypass. However, it is well known that the CO of the two sides of the heart is not identical because of the anatomic shunt between the systemic and pulmonary circulations, e.g., the bronchial artery. However, the difference between the flow rates was <3% of CO. Therefore, it is unlikely that such a minor difference in CO would influence the conclusion of this study.

Conclusion

We were able to characterize the venous return properties of the systemic and pulmonary circulations in a simple manner using the flat venous return surface. Equating the standard venous return surface with the measured integrated CO curves, under a variety of stressed blood volumes and cardiac functions, enabled us to accurately predict hemodynamics.

APPENDIX

Concept of Integrated Venous Return

Using a distributed model, Sagawa and Sunagawa and their coworkers (24, 30) modeled the vascular system. Suppose that compliance and resistance are distributed in the systemic circulation (Fig. 10). When the compliance distribution [$C(x)$] and pressure distribution [$P(x)$] are expressed as a function of distance (x) from the venous port, then stressed blood volume (V_S) in the systemic circulation can be described as

$$V_s = \int_0^L P(x)C(x)dx \qquad (A1)$$

where L represents the distance between the arterial and venous ports. If we denote the cumulative resistance over a distance x from the venous port by $R(x)$, the serial pressure distribution can be expressed as

$$P(x) = R(x)CO_V + P_{RA} \qquad (A2)$$

Substituting *Eq. A2* into *Eq. A1* yields

$$V_S = CO_V \int_0^L C(x)R(x)dx + P_{RA} \int_0^L C(x)dx \qquad (A3)$$

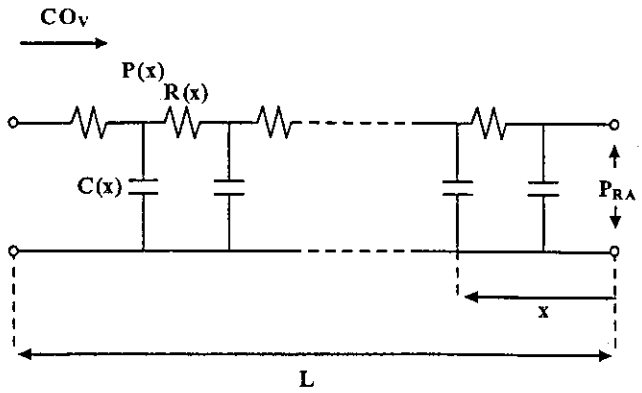

Fig. 10. Vascular system modeled by a distributed system. $C(x)$, $P(x)$, and $R(x)$, compliance, pressure, and cumulative resistance over a distance x from the venous port; L, distance between arterial and venous ports.

When $C_S D_{CS}(x)$ is substituted for $C(x)$, where C_S is the total systemic vascular compliance and $D_{CS}(x)$ is the normalized distribution of compliance as a function of x (thus $\int_0^L D_{CS}(x)dx$ is unity), *Eq. A3* can be rewritten as

$$V_S = CO_V C_S \int_0^L D_{CS}(x)R(x)dx + P_{RA}C_S \int_0^L D_{CS}(x)dx \qquad (A4)$$

The first integral term, which sums cumulative resistance weighted by systemic compliance distribution, is equivalent to the resistance for systemic venous return, R_{VS}, of Guyton et al. (16, 17). Because the second integral is unity, *Eq. A4* can be rewritten as

$$V_S = CO_V C_S R_{VS} + P_{RA}C_S \qquad (A5)$$

Stressed blood volume in the pulmonary circulation (V_P) can be related to CO_V and P_{LA} by the following equation

$$V_P = CO_V C_P R_{VP} + P_{LA}C_P \qquad (A6)$$

where C_P is the total pulmonary compliance and R_{VP} is the resistance for pulmonary venous return.

For a given condition, the sum of the stressed blood volumes in the systemic circulation and pulmonary circulation, V (i.e., $V_s + V_P$), remains constant, irrespective of its distribution. Thus adding *Eqs. A5* and *A6* and rearranging yields

$$CO_V = V/W - G_S P_{RA} - G_P P_{LA} \qquad (A7)$$

where W, G_S, and G_P are linear parameters and are expressed as

$$W = C_S R_{VS} + C_P R_{VP} \qquad (A8)$$

$$G_S = C_S/W \qquad (A9)$$

and

$$G_P = C_P/W \qquad (A10)$$

For a given V, CO_V can be related to P_{RA} and P_{LA} by a surface expressed by *Eq. A7* (Fig. 1*B*). When V is kept constant, CO_V decreases with increases in P_{RA} and/or P_{LA}.

From *Eqs. A8–A10*, once C_S, R_{VS}, C_P, and R_{VP} are given, we can estimate W, G_S, and G_P. Lee and Goldman (19) reported C_S as 1.9 $ml \cdot mmHg^{-1} \cdot kg^{-1}$ and R_{VS} as 0.056 $mmHg \cdot ml^{-1} \cdot min \cdot kg$ in eight dogs. Shoukas (26) reported C_P as 0.31 $ml \cdot mmHg^{-1} \cdot kg^{-1}$ and R_{VP} as 0.077 $mmHg \cdot ml^{-1} \cdot min \cdot kg$ in nine dogs. Estimated W, G_S, and G_P were 0.131 min, 14.56 $ml \cdot min^{-1} \cdot mmHg^{-1} \cdot kg^{-1}$, and 2.39 $ml \cdot min^{-1} \cdot mmHg^{-1} \cdot kg^{-1}$, respectively. These values are in good agreement with those obtained in our experiment.

ACKNOWLEDGMENTS

The authors gratefully acknowledge the technical assistance of Dr. Yoshiaki Takewa.

GRANTS

This study was supported by Japan Society for the Promotion of Science, Research, and Development Grant-In-Aid for Scientific Research C 14570707, a Ground-Based Research Grant for space utilization promoted by the National Space Development Agency of Japan and the Japan Space Forum, and the Program for Promotion of Fundamental Studies in Health Science of the Organization for Pharmaceutical Safety and Research of Japan.

REFERENCES

1. **Alexander RS.** Influence of constrictor drugs on the distensibility of the splanchnic venous system analyzed on the basis of an aortic model. *Circ Res* 2: 140–147, 1954.
2. **Braunwald E, Colucci WS, and Grossman W.** Clinical aspects of heart failure: high-output heart failure; pulmonary edema. In: *Heart Disease. A Textbook of Cardiovascular Medicine* (5th ed.), edited by Braunwald E. Philadelphia, PA: Saunders, 1997, p. 445–470.
3. **Brengelmann GL.** A critical analysis of the view that right atrial pressure determines venous return. *J Appl Physiol* 94: 849–859, 2003.
4. **Burkhoff D and Tyberg JV.** Why does pulmonary venous pressure rise after onset of LV dysfunction: a theoretical analysis. *Am J Physiol Heart Circ Physiol* 265: H1819–H1828, 1993.
5. **Caldini P, Permutt S, Waddell JA, and Riley RL.** Effect of epinephrine on pressure, flow, and volume relationships in the systemic circulation of dogs. *Circ Res* 34: 606–623, 1974.
6. **Chaliki HP, Hurrell DG, Nishimura RA, Reinke RA, and Appleton CP.** Pulmonary venous pressure: relationship to pulmonary artery, pulmonary wedge, and left atrial pressure in normal, lightly sedated dogs. *Catheter Cardiovasc Interv* 56: 432–438, 2002.
7. **Chen HI, Chang KC, and Hsieh KS.** Vascular factors in isovolumic systemic and pulmonary circuit. *Am J Physiol Heart Circ Physiol* 260: H201–H209, 1991.
8. **Den Hartog EA, Versprille A, and Jansen JR.** Systemic filling pressure in intact circulation determined on basis of aortic vs. central venous pressure relationships. *Am J Physiol Heart Circ Physiol* 267: H2255–H2258, 1994.
9. **Drees JA and Rothe CF.** Reflex venoconstriction and capacity vessel pressure-volume relationships in dogs. *Circ Res* 34: 360–73, 1974.
10. **Forrester JS, Diamond G, Chatterjee K, and Swan HJG.** Medical therapy of acute myocardial infarction by application of hemodynamic subsets. *N Engl J Med* 295: 1356–1362, 1976.
11. **Fuse K, Kodama M, Okura Y, Ito M, Hirono S, Kato K, Hanawa H, and Aizawa Y.** Predictors of disease course in patients with acute myocarditis. *Circulation* 102: 2829–2835, 2000.
12. **Glantz SA and Parmley WW.** Factors which affect the diastolic pressure-volume curve. *Circ Res* 42: 171–180, 1978.
13. **Grodins FS, Stuart WH, and Veenstra RL.** Performance characteristics of the right heart bypass preparation. *Am J Physiol* 198: 552–560, 1960.
14. **Guyton AC.** Determination of cardiac output by equating venous return curves with cardiac response curves. *Physiol Rev* 35: 123–129, 1955.
15. **Guyton AC, Jones CE, and Coleman TG.** *Circulatory Physiology: Cardiac Output and Its Regulation* (2nd ed.). Philadelphia, PA: Saunders, 1973, p. 237–252.
16. **Guyton AC, Lindsey AW, Abernathy B, and Richardson T.** Venous return at various right atrial pressures and the normal venous return curves. *Am J Physiol* 189: 609–615, 1957.
17. **Guyton AC, Lindsey AW, and Kaufmann BN.** Effect of mean circulatory filling pressure and other peripheral circulatory factors on cardiac output. *Am J Physiol* 180: 463–468, 1955.
18. **Harlan JC, Smith EE, and Richardson TQ.** Pressure-volume curves of systemic and pulmonary circuit. *Am J Physiol* 213: 1499–1503, 1967.
19. **Lee RW and Goldman S.** Mechanism for decrease in cardiac output with atrial natriuretic peptide in dogs. *Am J Physiol Heart Circ Physiol* 256: H760–H765, 1989.
20. **Levy MN.** The cardiac and vascular factors that determine systemic blood flow. *Circ Res* 44: 739–747, 1979.
21. **Lucas C, Johnson W, Hamilton MA, Fonarow GC, Woo MA, Flavell CM, Creaser JA, and Stevenson LW.** Freedom from congestion predicts good survival despite previous class IV symptoms of heart failure. *Am Heart J* 140: 840–847, 2000.
22. **Maughan WL, Sunagawa K, and Sagawa K.** Ventricular systolic interdependence: volume elastance model in isolated canine hearts. *Am J Physiol Heart Circ Physiol* 253: H1381–H1390, 1987.
23. **Ogilvie RI and Zborowska-Sluis D.** Effect of chronic rapid ventricular pacing on total vascular capacitance. *Circulation* 85: 1524–1530, 1992.
24. **Sagawa K, Maughan WL, Suga H, and Sunagawa K.** *Cardiac Contraction and Pressure-Volume Relationship.* Oxford, UK: Oxford Univ. Press, 1988, p. 232–298.
25. **Sarnoff SJ and Berglund E.** Ventricular function. 1. Starling's law of the heart, studied by means of simultaneous right and left ventricular function curves in the dog. *Circulation* 9: 706–718, 1953.
26. **Shoukas AA.** Pressure-flow and pressure-volume relations in the entire pulmonary vascular bed of the dog determined by two-port analysis. *Circ Res* 37: 809–818, 1975.

27. **Shoukas AA.** Carotid sinus baroreceptor reflex control and epinephrine. Influence on capacitive and resistive properties of the total pulmonary vascular bed of the dog. *Circ Res* 51: 95–101, 1982.
28. **Stone HL, Bishop VS, and Dong EJ.** Ventricular function in cardiac denervated and cardiac sympathectomized conscious dogs. *Circ Res* 20: 587–593, 1967.
29. **Sunagawa K, Maughan WL, Burkhoff D, and Sagawa K.** Left ventricular interaction with arterial load studied in isolated canine ventricle. *Am J Physiol Heart Circ Physiol* 245: H773–H780, 1983.
30. **Sunagawa K, Sagawa K, and Maughan WL.** Ventricular interaction with the loading system. *Ann Biomed Eng* 12: 163–189, 1984.
31. **Sylvester JT, Goldberg HS, and Permutt S.** The role of the vasculature in the regulation of cardiac output. *Clin Chest Med* 4: 111–126, 1983.
32. **Todaka K, Leibowitz D, Homma S, Fisher PE, Derosa C, Stennett R, Packer M, and Burkhoff D.** Characterizing ventricular mechanics and energetics following repeated coronary microembolization. *Am J Physiol Heart Circ Physiol* 272: H186–H194, 1997.
33. **Tyberg JV.** How changes in venous capacitance modulate cardiac output. *Pflügers Arch* 445: 10–17, 2002.
34. **Vatner SF and Braunwald E.** Cardiovascular control mechanisms in the conscious state. *N Engl J Med* 293: 970–976, 1975.
35. **Wang SY, Manyari DE, Scott-Douglas N, Smiseth OA, Smith ER, and Tyberg JV.** Splanchnic venous pressure-volume relation during experimental acute ischemic heart failure. Differential effects of hydralazine, enalaprilat, and nitroglycerin. *Circulation* 91: 1205–1212, 1995.

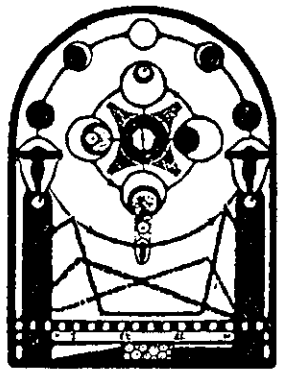

Am J Physiol Heart Circ Physiol 286: H1382–H1388, 2004.
First published November 20, 2003; 10.1152/ajpheart.00801.2003.

Muscle mechanoreflex induces the pressor response by resetting the arterial baroreflex neural arc

Kenta Yamamoto,[1] Toru Kawada,[1] Atsunori Kamiya,[1] Hiroshi Takaki,[1] Tadayoshi Miyamoto,[1,2] Masaru Sugimachi,[1] and Kenji Sunagawa[1]

[1]*Department of Cardiovascular Dynamics, National Cardiovascular Center Research Institute, Osaka 565-8565; and* [2]*Japan Association for the Advancement of Medical Equipment, Tokyo 113-0033, Japan*

Submitted 29 August 2003; accepted in final form 19 November 2003

Yamamoto, Kenta, Toru Kawada, Atsunori Kamiya, Hiroshi Takaki, Tadayoshi Miyamoto, Masaru Sugimachi, and Kenji Sunagawa. Muscle mechanoreflex induces the pressor response by resetting the arterial baroreflex neural arc. *Am J Physiol Heart Circ Physiol* 286: H1382–H1388, 2004. First published November 20, 2003; 10.1152/ajpheart.00801.2003.—The effects of the muscle mechanoreflex on the arterial baroreflex neural control have not previously been analyzed over the entire operating range of the arterial baroreflex. In anesthetized, vagotomized, and aortic-denervated rabbits (n = 8), we isolated carotid sinuses and changed intracarotid sinus pressure (CSP) from 40 to 160 mmHg in increments of 20 mmHg every minute while recording renal sympathetic nerve activity (SNA) and arterial pressure (AP). Muscle mechanoreflex was induced by passive muscle stretch (5 kg of tension) of the hindlimb. Muscle stretch shifted the CSP-SNA relationship (neural arc) to a higher SNA, whereas it did not affect the SNA-AP relationship (peripheral arc). SNA was almost doubled [from 63 ± 15 to 118 ± 14 arbitrary units (au), $P < 0.05$] at the CSP level of 93 ± 8 mmHg, and AP was increased ~50% by muscle stretch. When the baroreflex negative feedback loop was closed, muscle stretch increased SNA from 63 ± 15 to 81 ± 21 au ($P < 0.05$) and AP from 93 ± 8 to 109 ± 12 mmHg ($P < 0.05$). In conclusion, the muscle mechanoreflex resets the neural arc to a higher SNA, which moves the operating point towards a higher SNA and AP under baroreflex closed-loop conditions. Analysis of the baroreflex equilibrium diagram indicated that changes in the neural arc induced by the muscle mechanoreflex might compensate for pressure falls resulting from exercise-induced vasodilatation.

sympathetic nerve activity; arterial pressure; baroreflex equilibrium diagram; exercise pressor reflex; exercise

THE ARTERIAL BAROREFLEX plays an important role in stabilization of arterial pressure (AP) during daily activity. The input-output relationship of the arterial baroreflex system between baroreceptor pressure input and the resultant AP approximates a sigmoidal stimulus-response curve (19). This stimulus-response curve is known to reset toward a higher AP during exercise (7, 8, 23, 24, 29, 30, 34, 35). Recently, it was reported that exercise shifted the baroreflex curve for sympathetic nerve activity (SNA) to a higher SNA (5, 26). However, the neural mechanism responsible for the changes in baroreflex during exercise remains unclear. During exercise, AP and SNA are regulated by central command and the exercise pressor reflex (15, 22, 27, 42). The exercise pressor reflex is evoked by afferent inputs from metabolic (muscle metaboreflex)- and mechanical (muscle mechanoreflex)-sensitive skeletal muscle receptors. The muscle mechanoreflex has a dominant role in the exercise pressor reflex (6, 9, 20). We therefore hypothesized that the muscle mechanoreflex would reset the carotid sinus baroreflex control of SNA toward a higher SNA, evoking a pressor response under baroreflex closed-loop conditions. Earlier studies have reported that the muscle mechanoreflex reset the arterial baroreflex for AP and/or heart rate (13, 32). In the present study, we aimed to quantitatively investigate the effect of the muscle mechanoreflex on the carotid sinus baroreflex control of SNA.

Although the neural mechanism involved in resetting the baroreflex may be best analyzed using the baroreflex equilibrium diagram (28, 38), to the best of our knowledge, the effects of the muscle mechanoreflex on baroreflex function have never been assessed using this method. The baroreflex equilibrium diagram consists of the neural and peripheral arcs. The neural arc represents the static input-output relationship between baroreceptor pressure input and SNA, and the peripheral arc represents the relationship between SNA and AP. The intersection of the neural and peripheral arcs defines the operating point of the AP regulation under baroreflex closed-loop conditions (see *Theoretical considerations: coupling of neural and peripheral arcs* in MATERIALS AND METHODS for details).

To construct the baroreflex equilibrium diagram, we performed an open-loop experiment on the carotid sinus baroreflex in anesthetized rabbits (16–18, 38). The muscle mechanoreflex was induced by passive muscle stretch of the triceps surae muscle. The results of the present study indicate that the muscle mechanoreflex resets the baroreflex neural arc to a higher SNA, moving the operating point toward a higher AP under baroreflex closed-loop conditions.

MATERIALS AND METHODS

Theoretical considerations: coupling of neural and peripheral arcs. Changes in AP are immediately sensed by arterial baroreceptors, which alter efferent SNA via the arterial baroreflex. Efferent SNA, in turn, governs heart rate and the mechanical properties of the heart and vessels, which themselves exert a direct influence over AP. This cyclical negative feedback makes it difficult to analyze the behavior of the arterial baroreflex. To overcome this problem, we opened the negative feedback loop and divided the system into controlling and controlled elements (28). We defined the controlling element as a neural arc and the controlled element as a peripheral arc. In the neural arc, the input is the pressure sensed by the arterial baroreceptors and the output is SNA. In the peripheral arc, the input is SNA and the output is AP. Because pressure sensed by the arterial baroreceptor is

Address for reprint requests and other correspondence: K. Yamamoto, Dept. of Cardiovascular Dynamics, National Cardiovascular Center Research Institute, 5-7-1 Fujishirodai, Suita, Osaka 565-8565, Japan (E-mail: kentay@ri.ncvc.go.jp).

The costs of publication of this article were defrayed in part by the payment of page charges. The article must therefore be hereby marked "*advertisement*" in accordance with 18 U.S.C. Section 1734 solely to indicate this fact.

equilibrated with AP under physiological conditions, we superimposed the functions of the two arcs and determined the operating point of the system from the intersection of the two arcs. The operating point is defined as the AP and SNA under closed-loop conditions of the feedback system. The validity of this framework has been examined in a previous study (38). Using the baroreflex equilibrium diagram, we aimed to quantify the effects of the muscle mechanoreflex on the carotid sinus baroreflex.

Surgical preparations. Animals were cared for in strict accordance with the Guiding Principles for the Care and Use of Animals in the Field of Physiological Sciences approved by the Physiological Society of Japan. Japanese White rabbits weighing 2.3–3.1 kg were anesthetized via an intravenous injection (2 ml/kg) with a mixture of urethane (250 mg/ml) and α-chloralose (40 mg/ml) and mechanically ventilated with oxygen-enriched room air. Arterial blood was sampled from the left common carotid artery. The rabbits were slightly hyperventilated to suppress chemoreflexes (arterial P_{CO_2} ranged from 30 to 35 mmHg, arterial $P_{O_2} > 300$ mmHg). Arterial blood pH was within the physiological range when rabbits were examined at the end of the surgical preparation and also at the end of the experiment. Supplemental anesthetics were administered continuously to maintain an appropriate level of anesthesia (0.3 $ml \cdot kg^{-1} \cdot h^{-1}$). The body temperature of each animal was maintained at ~38°C with a heating pad. AP was measured using a high-fidelity pressure transducer (Millar Instruments; Houston, TX) inserted retrogradely from the right common carotid artery to the aortic arch.

We isolated the bilateral carotid sinuses from the systemic circulation by ligating the internal and external carotid arteries and other small branches originating from the carotid sinus region. The isolated carotid sinuses were filled with warmed physiological saline via catheters inserted through the common carotid arteries. Intracarotid sinus pressure (CSP) was controlled by a servo-controlled piston pump (model ET-126A, Labworks; Costa Mesa, CA). Bilateral vagal and aortic depressor nerves were sectioned at the neck to eliminate baroreflexes from the cardiopulmonary region and aortic arch.

We exposed the left renal sympathetic nerve retroperitoneally and attached a pair of stainless steel wire electrodes (Bioflex wire AS633, Cooner Wire) to record SNA. The nerve bundle peripheral to the electrodes was tightly ligated and crushed to eliminate afferent signals from the kidney. The nerve and electrodes were secured with silicone glue (Kwik-Sil, World Precision Instruments; Sarasota, FL). The preamplified nerve signal was band-pass filtered at 150–1,000 Hz. It was then full-wave rectified and low-pass filtered with a cutoff frequency of 30 Hz to quantify the nerve activity. Pancuronium bromide (0.1 mg/kg) was administered to prevent contamination of SNA recordings by muscular activity.

With the rabbit in the prone position, the sacrum and the left ankle were clamped with a custom-made apparatus to prevent body trunk and hindlimb movement during muscle stretch. The left triceps surae muscle, Achilles tendon, and calcaneus bone were exposed. The left triceps surae muscle was isolated from surrounding tissue. The Achilles tendon was severed from the calcaneus bone and attached to a force transducer (Load Cell LUR-A-SA1, Kyowa Electronic Instruments; Tokyo, Japan). During muscle stretch, the force transducer was also connected to a 5-kg weight via a pulley, which opposed the Achilles tendon.

Protocols. Fourteen rabbits were used in the present study. Two rabbits were subjected to both *protocols 1* and *2* as described below.

In *protocol 1*, we examined the time course of the SNA response to stepwise muscle stretch ($n = 8$). Before muscle stretch, CSP was adjusted to instantaneous AP, and the operating point was determined from mean AP at steady state. CSP was then fixed at the operating point, and the left triceps surae muscle was stretched at 5 kg for 7 min.

In *protocol 2a*, we obtained the baroreflex equilibrium diagram under both control and muscle stretch conditions ($n = 8$). CSP was first decreased to 40 mmHg. After attainment of a steady state, CSP was then increased from 40 to 160 mmHg in increments of 20 mmHg. Each pressure step was maintained for 60 s. When SNA was completely suppressed and AP had fallen below 50 mmHg at the CSP level of 140 mmHg, the CSP level of 160 mmHg was omitted to prevent deterioration of the animal's condition. Thus the maximum duration of muscle stretch was 7 min. The order of control and muscle stretch conditions was randomized across the animals. In five of eight animals, the estimation of the baroreflex equilibrium diagram was repeated under both control and muscle stretch conditions after the left tibial nerve was severed.

In *protocol 2b*, we measured the actual operating point in the same eight animals that were used in *protocol 2a* to determine the accuracy of the operating point derived from the baroreflex equilibrium diagram. The operating point of the carotid sinus baroreflex was defined as the point where CSP equals AP (38). To obtain the actual operating point, CSP was adjusted to match AP via the servo-controlled system so that the carotid sinus baroreflex was virtually closed. After a steady state was reached, mean AP (and thus CSP) and SNA were taken as the values defining the actual operating point under control conditions. We also performed muscle stretch for 1 min while the carotid sinus baroreflex was virtually closed and obtained mean AP and SNA values defining the actual operating point during the last 10 s of muscle stretch.

Data analysis. We recorded CSP, SNA, and AP at a sampling rate of 200 Hz using a 12-bit analog-to-digital converter. Data were stored on the hard drive of a dedicated laboratory computer system for later analyses.

In *protocol 2a*, we calculated mean SNA and AP during the last 10 s of each CSP step. Because the absolute magnitude of SNA depended on recording conditions, SNA was presented in arbitrary units (au) so that the minimum and maximum values of SNA data obtained under control conditions were set to zero and 100 au, respectively, for each animal. A four-parameter logistic function analysis was performed on the neural arc (CSP-SNA data pairs) and the peripheral arc (SNA-AP data pairs) as follows (19)

$$y = \frac{P_1}{1 + \exp[P_2(x - P_3)]} + P_4 \quad (1)$$

where x and y represent the input and the output, respectively; P_1 denotes the response range (i.e., the difference between the maximum and minimum values of y); P_2 is the coefficient of gain; P_3 defines the midpoint of the logistic function on the input axis; and P_4 represents the minimum value of y. The maximum gain (G_{max}) is $-P_1P_2/4$ at $x = P_3$.

In *protocol 2b*, we measured the actual operating point by closing the arterial baroreflex negative feedback loop. Mean SNA and AP values were obtained by averaging 10-s data at the steady state under both control and muscle stretch conditions.

Statistical analysis. All data are presented as means ± SD. Differences were considered significant when $P < 0.05$. The effects of muscle stretch on the parameters of the neural and peripheral arcs and operating points were examined using the paired t-test. The operating point as determined from the equilibrium diagram (*protocol 2a*) was compared with the operating point actually measured (*protocol 2b*) using linear regression analysis.

RESULTS

Figure 1 shows the group-averaged step response of SNA to muscle stretch. These data were collected under baroreflex open-loop conditions where CSP was fixed at an operating point of each animal. CSP was 87 ± 14 mmHg across all the animals. Muscle stretch transiently decreased and then increased SNA. The SNA value at 7 min was maintained at 93 ± 9% of the SNA at 1 min.

Figure 2 shows a typical time series of CSP, SNA, and AP under control conditions (*left*) and muscle stretch conditions

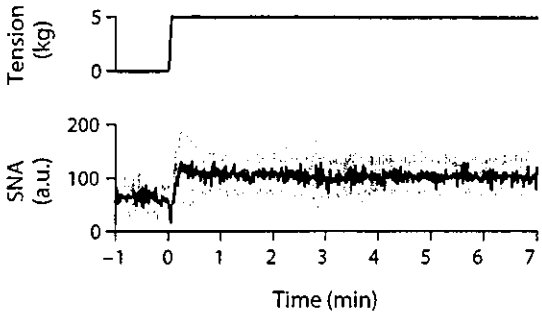

Fig. 1. Step response of sympathetic nerve activity [SNA; in arbitrary units (au)] to muscle stretch obtained from *protocol 1*. SNA transiently decreased and then increased during muscle stretch. The SNA response reached a steady state within ~40 s. The SNA value at 7 min was maintained at 93 ± 9% of the value observed at 1 min. The solid line indicates the mean value and the gray area represents means ± SD. Data were resampled at 1 Hz.

(*right*) obtained from *protocol 2a*. SNA and AP decreased in response to the increments in CSP under both control and muscle stretch conditions. Muscle stretch increased SNA and AP at CSP levels up to 100 mmHg in this animal.

Figure 3 illustrates the baroreflex neural arcs (*A*) and peripheral arcs (*B*) derived from the same data employed in Fig. 2. The open and closed circles represent data points obtained under control and muscle stretch conditions, respectively. The thin and thick solid lines indicate the fitted logistic functions under control and muscle stretch conditions, respectively. In the neural arcs, SNA decreased in response to the increments in CSP under both conditions. Muscle stretch increased SNA at CSP levels up to 100 mmHg. In the peripheral arcs, AP positively correlated with SNA. Peripheral arcs obtained under both conditions were nearly identical.

Figure 3*C* depicts the baroreflex equilibrium diagrams combined from Fig. 3, *A* and *B*. The thin and thick solid lines indicate the fitted logistic functions under control and muscle stretch conditions, respectively. Because CSP is equilibrated with AP under physiological conditions, the operating point is determined from the intersection of the neural and peripheral arcs. Muscle stretch moved the operating point toward higher SNA and AP (from *point a* to *point b*).

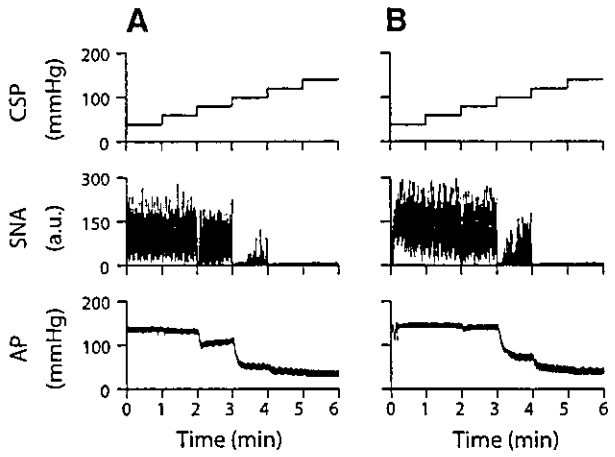

Fig. 2. Typical time series of intracarotid sinus pressure (CSP), SNA, and arterial pressure (AP) under control conditions (*A*) and muscle stretch conditions (*B*) obtained from *protocol 2a*. Data were resampled at 10 Hz. SNA and AP decreased in response to increments in CSP under both control and muscle stretch conditions. Muscle stretch increased SNA and AP at CSP levels up to 100 mmHg in this animal.

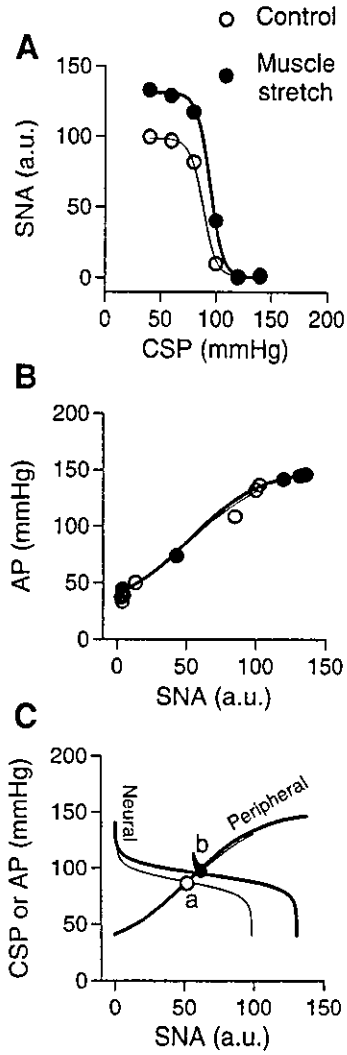

Fig. 3. Baroreflex neural arcs (*A*), peripheral arcs (*B*), and baroreflex equilibrium diagrams (*C*). In the neural (*A*) and peripheral arcs (*B*), the open and closed circles represent data points obtained under control and muscle stretch conditions, respectively. The thin and thick solid lines indicate fitted logistic functions under control and muscle stretch conditions, respectively. Muscle stretch increased SNA at CSP levels up to 100 mmHg in the neural arc. The peripheral arcs under both conditions were nearly identical. In baroreflex equilibrium diagrams (*C*), the thin and thick solid lines indicate fitted logistic functions under control and muscle stretch conditions, respectively. Because CSP is equilibrated with AP under physiological conditions, the operating point is determined from the intersection of the neural and peripheral arcs. Muscle stretch moved the operating point toward a higher AP (from *point a* to *point b*).

Figure 4*A* illustrates the role of the baroreflex function during muscle stretch and is derived from representative data from one animal. Muscle stretch almost doubled SNA from 54 to 98 au at the CSP level of the control operating point (*point a*), resulting in an elevation in AP of ~50%, from 87 to 130 mmHg (*point c*). When the arterial baroreflex was operative, the increases in SNA and AP recorded during muscle stretch were substantially attenuated (*point b*).

Figure 4*B* shows the group-averaged CSP, SNA, and AP obtained from eight animals under control and muscle stretch conditions at the CSP level of 93 ± 8 mmHg (control operating

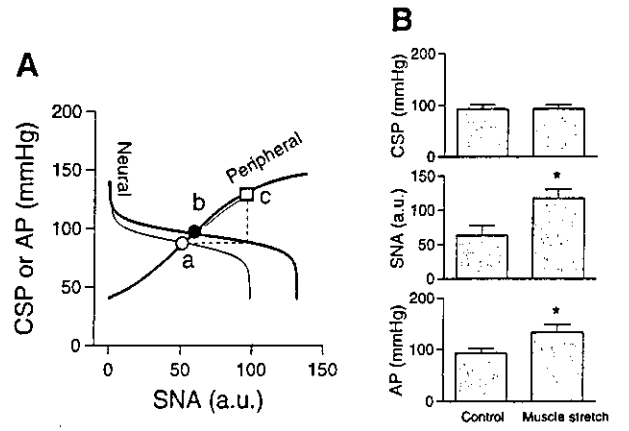

Fig. 4. *A*: role of the baroreflex function during muscle stretch derived from representative data from one animal. The thin and thick solid lines indicate the baroreflex equilibrium diagram under control and muscle stretch conditions, respectively. *Points a* and *b* represent the operating points under baseline and muscle stretch conditions, respectively. In instances where changes in AP during muscle stretch were not sensed by the arterial baroreflex, SNA would increase to ~100 au, resulting in elevation of AP above ~130 mmHg (*point c*). *B*: group-averaged CSP, SNA, and AP obtained from 8 animals under control and muscle stretch conditions at the CSP level of 93 ± 8 mmHg (control operating point). Muscle stretch nearly doubled the SNA, indicating that muscle stretch shifted the neural arc to SNA levels approximately twice at the CSP level of the control operating point. The twofold increase in SNA induced an AP elevation of ~50% at the same CSP level. *$P < 0.05$ from control.

point). Muscle stretch nearly doubled SNA, indicating that the muscle stretch shifted the neural arc to SNA values approximately twice those at the CSP level of the control operating point. This twofold increase in SNA induced an AP elevation of ~50% at the same CSP level.

The group-averaged parameters of the neural and peripheral arcs are summarized in Table 1. In the neural arc, the response range of SNA (P_1) and the midpoint of the operating range (P_3) were increased by muscle stretch. The coefficient of gain (P_2) and the minimum value of SNA (P_4) did not differ between control and muscle stretch conditions. G_{max} was increased by muscle stretch. In the peripheral arc, muscle stretch did not affect any of the four parameters or G_{max}. Muscle stretch significantly increased both AP and SNA at the operating point estimated from the baroreflex equilibrium diagram. A supplementary experiment associated with *protocol 2a* demonstrated that the effects of muscle stretch on the neural arc were abolished by tibial denervation (Table 2).

In *protocol 2b*, the actual operating point was measured by closing the baroreflex negative feedback loop. Muscle stretch increased AP from 92 ± 8 to 109 ± 14 mmHg ($P < 0.05$) and SNA from 61 ± 11 to 84 ± 25 au ($P < 0.05$) at the operating point. Figure 5 shows the relationship between the operating point estimated from the equilibrium diagram and that measured in eight animals. Each animal provided two data points determined under control and muscle stretch conditions (16 data points in total). For both AP and SNA, the estimated values were similar to the measured results. Root mean square errors of estimate were 4% for AP and 11% for SNA.

Table 1. *Effect of muscle stretch on the neural and peripheral arc parameters and operating point*

	Control	Muscle Stretch
Neural arc		
P_1, au	98.7±4.0	132.6±16.0*
P_2, au/mmHg	0.12±0.04	0.13±0.03
P_3, mmHg	104±11	109±11*
P_4, au	0.1±2.3	5.2±9.2
G_{max} au/mmHg	−2.9±0.9	−4.4±0.9*
Peripheral arc		
P_1, mmHg	118±30	118±10
P_2, au/mmHg	−0.05±0.02	−0.04±0.01
P_3, au	67.5±24.3	71.4±28.3
P_4, mmHg	30±11	34±7
G_{max}, au/mmHg	1.3±0.3	1.3±0.4
Values at operating point		
AP, mmHg	93±8	109±12*
SNA, au	63.1±15.1	81.2±21.0*

Values are means ± SD; $n = 8$ animals. See *Eq. 1* for definitions of the four parameters of logistic function (P_1–P_4). G_{max}, maximum gain. *$P < 0.05$ from control.

DISCUSSION

The key new findings of the present study are as follows. Muscle stretch reset the carotid sinus baroreflex neural arc to a higher SNA. In contrast, muscle stretch did not affect the baroreflex peripheral arc. As a result, the operating point determined from the intersection of the neural and peripheral arcs moved toward a higher AP during muscle stretch. These results support the hypothesis that the muscle mechanoreflex induces the pressor response by resetting the arterial baroreflex neural arc.

Interaction between the muscle mechanoreflex and arterial baroreflex. Although Potts and Li (31) showed that elevation of CSP attenuated the pressor response induced by muscle stretch, they did not measure SNA in that study. Our study demonstrated that the muscle mechanoreflex shifted the CSP-SNA curve toward a higher SNA primarily at low and midrange CSP readings (Fig. 3 and Table 1). This was not an outcome of the time-dependent changes in the muscle stretch effect, because the muscle stretch produced a sustained SNA increase for at least 7 min (Fig. 1). These results suggest that the baroreceptor input pressure-dependent pressor response due to muscle stretch is a consequence of the neural interaction between the muscle mechanoreflex and arterial baroreflex.

Miki et al. (26) demonstrated that treadmill exercise shifted the relationship between baroreceptor pressure input and SNA to a higher SNA. The shift in the baroreflex neural arc evoked by the muscle mechanoreflex may contribute to the exercise-induced resetting in the baroreflex control of SNA. Further-

Table 2. *Effect of muscle stretch after severing of the nerve supply to the hindlimb muscles on parameters of logistic function analysis for the neural arc*

	Control	Muscle Stretch
Neural arc		
P_1 au	99.5±2.1	100.8±8.2
P_2, au/mmHg	0.12±0.03	0.11±0.02
P_3, mmHg	107±5	110±8
P_4, au	0.3±1.6	0.2±3.7
G_{max}, au/mmHg	−2.9±0.7	−2.8±0.6

Values are means ± SD; $n = 5$ animals.

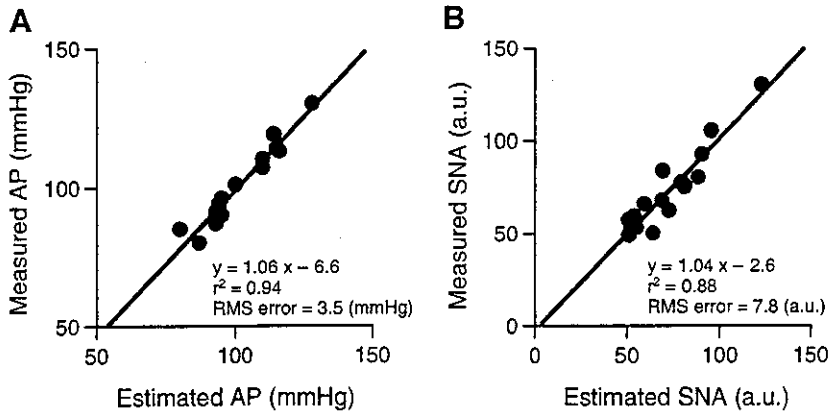

Fig. 5. Relationship between the operating point estimated from the equilibrium diagram and operating point actually measured in 8 animals. Each animal provided two data points determined under control and muscle stretch conditions (16 data points in total). The operating point estimated by the baroreflex equilibrium diagram matched the value obtained from actual measurements. *A*: measured vs. estimated AP; *B*: measured vs. estimated SNA. RMS, root mean square.

more, G_{max} of the neural arc (the CSP-SNA relationship) was increased by muscle stretch when the data were analyzed using a fitted logistic function (*Eq. 1*). The present result is consistent with previous studies (14, 26) showing that gain in the arterial baroreflex control of vascular sympathetic outflow was increased during static and dynamic exercise. On the other hand, another study showed no changes in the gain of the carotid sinus baroreflex control of SNA during dynamic arm exercise (5). Whether changes in the neural arc gain depend on the intensity and/or modality of exercise awaits further studies.

Previous studies (1, 40) suggest interactions between the muscle mechanoreflex and the arterial baroreflex in the brain stem. Baroreceptor afferent inputs inhibit neurons in the rostral ventrolateral medulla (RVLM). Electrically induced muscle contraction increases the firing frequency in RVLM neurons (2, 3), suggesting that the baroreflex and muscle mechanoreflex share common central pathways. In addition, the contraction-sensitive muscle afferents inhibit the baroreflex signal transduction through activation of GABA receptors in the nucleus tractus solitarii (33). This neural integration in the brainstem may be involved in the resetting of the arterial baroreflex neural arc induced by the muscle mechanoreflex.

Determination of the operating point of the arterial baroreflex. SNA and AP during muscle stretch may be determined via interactions between the muscle mechanoreflex and the arterial baroreflex. Muscle stretch shifted the neural arc to SNA values approximately double at the CSP level derived from the control operating point, whereas it did not affect the peripheral arc (Table 1 and Figs. 3 and 4). As a result, the operating point derived from the intersection of the two arcs moved toward a higher AP (Fig. 3*C*). These findings suggest that resetting in the neural arc, rather than in the peripheral arc, is responsible for the increases in SNA and AP during muscle stretch observed under baroreflex closed-loop conditions (21, 41). These data are the first to provide quantitative evidence demonstrating that resetting of the carotid sinus baroreflex (via central resetting of the baroreflex neural arc) is necessary to evoke the sympathoexcitatory and pressor responses associated with activation of mechanosensitive afferents in the closed-loop conditions.

The baroreflex equilibrium diagram is useful for intuitive understanding of the cardiovascular controls (28, 38). Figure 4*A* illustrates the role of the baroreflex function during muscle stretch. The baseline operating point was determined from the intersection of the neural and peripheral arcs (*point a*). Muscle stretch reset the neural arc from the thin line to the thick line. If changes in AP were not sensed by the arterial baroreflex, then muscle stretch nearly doubled SNA, resulting in AP elevation above ~130 mmHg (*point c*). However, when the arterial baroreflex was operative, the increases in SNA and AP during the muscle stretch were substantially attenuated (*point b*).

Sato et al. (38) demonstrated that the actual operating point matched the intersection of the neural and peripheral arcs under both control and hemorrhagic conditions. In the present study, the operating point estimated from the equilibrium diagram was in close agreement with that actually measured under both control and muscle stretch conditions (Fig. 5). These results confirm the accuracy of the operating point estimation derived from the equilibrium diagram.

Physiological implications. Dynamic exercise causes only a modest rise in mean AP despite a marked sympathoexcitation (36). This phenomenon is believed to be a consequence of the decreased sympathetic constrictor response due to metabolic vasodilation and sympatholysis in exercising muscles (4, 11, 12, 37). Figure 6 illustrates a putative diagram of the arterial baroreflex control of SNA and AP during the dynamic exercise. The muscle mechanoreflex resets the neural arc to a higher SNA. Vasodilation in exercising muscles presumably shifts the peripheral arc downward. If the neural arc is not reset to a higher SNA during dynamic exercise, AP at the operating point might decrease (*point c*) relative to that observed under resting conditions (*point a*). However, by resetting the neural

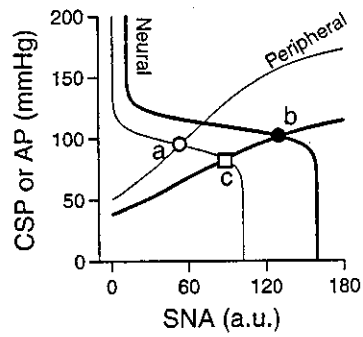

Fig. 6. Putative diagram of the arterial baroreflex controls of SNA and AP during dynamic exercise. Thin solid lines indicate the baroreflex equilibrium diagram under resting conditions. Thick solid lines indicate the baroreflex equilibrium diagram during dynamic exercise. *Points a* and *b* represent the operating points at rest and during exercise, respectively. If the neural arc did not reset to a higher SNA during dynamic exercise, then AP at the operating point would decrease (*point c*).

arc, AP may be maintained against the downward shift in the peripheral arc (*point b*). Thus we speculate that resetting of the neural arc induced by the muscle mechanoreflex contributes to maintaining AP despite the downward shift of the peripheral arc due to vasodilation in exercising muscles.

In the present study, we did not examine additional factors that may potentially influence SNA and AP regulation such as central command, muscle metaboreflex, and vasodilation in exercising muscles. Further investigations are required to improve our understanding of the arterial baroreflex control of SNA and AP during exercise.

Limitations. The present study has several limitations. First, we performed the experiment in animals under anesthetized conditions. Although anesthesia was convenient for elimination of the central command, the gain of carotid baroreflex and muscle mechanoreflex might have been estimated differently if the animals had been conscious.

Second, we used passive muscle stretch as the input for the muscle mechanoreflex. The shift in the baroreflex neural arc was abolished by the tibial denervation (Table 2), suggesting that the shift was evoked by the neural afferents from hindlimb muscles. Previous studies (10, 25, 39) have suggested that passive muscle stretch selectively activates muscle mechanoreceptors. Thus we believe that muscle stretch had evoked the muscle mechanoreflex in the present study.

In conclusion, the muscle mechanoreflex resets the arterial baroreflex neural arc to a higher SNA. Consequently, the pressor response is evoked during muscle stretch under baroreflex closed-loop conditions. This shift in the neural arc induced by the muscle mechanoreflex might compensate for AP falls resulting from exercise-induced vasodilatation.

GRANTS

This study was supported by Ministry of Health Labour and Welfare of Japan Health and Labour Sciences Research Grant for Research on Advanced Medical Technology 13090401 (H14-Nano-002), by Japan Society for the Promotion of Science Grant-in-Aid for Scientific Research (A) 15200040, and by the Program for Promotion of Fundamental Studies in Health Science of the Organization for Pharmaceutical Safety and Research of Japan.

REFERENCES

1. **Aicher SA, Kurucz OS, Reis DJ, and Milner TA.** Nucleus tractus solitarius efferent terminals synapse on neurons in the caudal ventrolateral medulla that project to the rostral ventrolateral medulla. *Brain Res* 693: 51–63, 1995.
2. **Bauer RM, Iwamoto GA, and Waldrop TG.** Discharge patterns of ventrolateral medullary neurons during muscular contraction. *Am J Physiol Regul Integr Comp Physiol* 259: R606–R611, 1990.
3. **Bauer RM, Waldrop TG, Iwamoto GA, and Holzwarth MA.** Properties of ventrolateral medullary neurons that respond to muscular contraction. *Brain Res Bull* 28: 167–178, 1992.
4. **Buckwalter JB, Naik JS, Valic Z, and Clifford PS.** Exercise attenuates α-adrenergic receptor responsiveness in skeletal muscle vasculature. *J Appl Physiol* 90: 172–178, 2001.
5. **Fadel PJ, Ogoh S, Watenpaugh DE, Wasmund W, Olivencia-Yurvati A, Smith ML, and Raven PB.** Carotid baroreflex regulation of sympathetic nerve activity during dynamic exercise in humans. *Am J Physiol Heart Circ Physiol* 280: H1383–H1390, 2001.
6. **Gallagher KM, Fadel PJ, Smith SA, Norton KH, Querry RG, Olivencia-Yurvati A, and Raven PB.** Increases in intramuscular pressure raise arterial blood pressure during dynamic exercise. *J Appl Physiol* 91: 2351–2358, 2001.
7. **Gallagher KM, Fadel PJ, Stromstad M, Ide K, Smith SA, Querry RG, Raven PB, and Secher NH.** Effects of exercise pressor reflex activation on carotid baroreflex function during exercise in humans. *J Physiol* 533: 871–880, 2001.
8. **Gallagher KM, Fadel PJ, Stromstad M, Ide K, Smith SA, Querry RG, Raven PB, and Secher NH.** Effects of partial neuromuscular blockade on carotid baroreflex function during exercise in humans. *J Physiol* 533: 861–870, 2001.
9. **Hayes SG and Kaufman MP.** Gadolinium attenuates exercise pressor reflex in cats. *Am J Physiol Heart Circ Physiol* 280: H2153–H2161, 2001.
10. **Hayes SG and Kaufman MP.** MLR stimulation and exercise pressor reflex activate different renal sympathetic fibers in decerebrate cats. *J Appl Physiol* 92: 1628–1634, 2002.
11. **Howard MG and DiCarlo SE.** Reduced vascular responsiveness after a single bout of dynamic exercise in the conscious rabbit. *J Appl Physiol* 73: 2662–2667, 1992.
12. **Howard MG, DiCarlo SE, and Stallone JN.** Acute exercise attenuates phenylephrine-induced contraction of rabbit isolated aortic rings. *Med Sci Sports Exerc* 24: 1102–1107, 1992.
13. **Iellamo F, Legramante JM, Raimondi G, and Peruzzi G.** Baroreflex control of sinus node during dynamic exercise in humans: effects of central command and muscle reflexes. *Am J Physiol Heart Circ Physiol* 272: H1157–H1164, 1997.
14. **Kamiya A, Michikami D, Fu Q, Niimi Y, Iwase S, Mano T, and Suzumura A.** Static handgrip exercise modifies arterial baroreflex control of vascular sympathetic outflow in humans. *Am J Physiol Regul Integr Comp Physiol* 281: R1134–R1139, 2001.
15. **Kaufman MP and Forster HV.** Reflexes controlling circulatory, ventilatory and airway responses to exercise. In: *Handbook of Physiology. Exercise: Regulation and Integration of Multiple Systems. Control of Respiratory and Cardiovascular Systems.* Bethesda, MD: Am. Physiol. Soc., 1996, sect. 12, pt. II, chapt. 10, p. 381–447.
16. **Kawada T, Shishido T, Inagaki M, Tatewaki T, Zheng C, Yanagiya Y, Sugimachi M, and Sunagawa K.** Differential dynamic baroreflex regulation of cardiac and renal sympathetic nerve activities. *Am J Physiol Heart Circ Physiol* 280: H1581–H1590, 2001.
17. **Kawada T, Shishido T, Inagaki M, Zheng C, Yanagiya Y, Uemura K, Sugimachi M, and Sunagawa K.** Estimation of baroreflex gain using a baroreflex equilibrium diagram. *Jpn J Physiol* 52: 21–29, 2002.
18. **Kawada T, Uemura K, Kashihara K, Jin Y, Li M, Zheng C, Sugimachi M, and Sunagawa K.** Uniformity in dynamic baroreflex regulation of left and right cardiac sympathetic nerve activities. *Am J Physiol Regul Integr Comp Physiol* 284: R1506–R1512, 2003.
19. **Kent BB, Drane JW, Blumenstein B, and Manning JW.** A mathematical model to assess changes in the baroreceptor reflex. *Cardiology* 57: 295–310, 1972.
20. **Leshnower BG, Potts JT, Garry MG, and Mitchell JH.** Reflex cardiovascular responses evoked by selective activation of skeletal muscle ergoreceptors. *J Appl Physiol* 90: 308–316, 2001.
21. **Matsukawa K, Wall PT, Wilson LB, and Mitchell JH.** Reflex responses of renal nerve activity during isometric muscle contraction in cats. *Am J Physiol Heart Circ Physiol* 259: H1380–H1388, 1990.
22. **McCloskey DI and Mitchell JH.** Reflex cardiovascular and respiratory responses originating in exercising muscle. *J Physiol* 224: 173–186, 1972.
23. **McIlveen SA, Hayes SG, and Kaufman MP.** Both central command and exercise pressor reflex reset carotid sinus baroreflex. *Am J Physiol Heart Circ Physiol* 280: H1454–H1463, 2001.
24. **Melcher A and Donald DE.** Maintained ability of carotid baroreflex to regulate arterial pressure during exercise. *Am J Physiol Heart Circ Physiol* 241: H838–H849, 1981.
25. **Mense S and Stahnke M.** Responses in muscle afferent fibres of slow conduction velocity to contractions and ischaemia in the cat. *J Physiol* 342: 383–397, 1983.
26. **Miki K, Yoshimoto M, and Tanimizu M.** Acute shifts of baroreflex control of renal sympathetic nerve activity induced by treadmill exercise in rats. *J Physiol* 548: 313–322, 2003.
27. **Mitchell JH, Kaufman MP, and Iwamoto GA.** The exercise pressor reflex: its cardiovascular effects, afferent mechanisms, and central pathways. *Annu Rev Physiol* 45: 229–242, 1983.
28. **Mohrman DE and Heller LJ.** *Cardiovascular Physiology* (4th ed.). New York: McGraw-Hill, 1997, p. 158–230.
29. **Norton KH, Boushel R, Strange S, Saltin B, and Raven PB.** Resetting of the carotid arterial baroreflex during dynamic exercise in humans. *J Appl Physiol* 87: 332–338, 1999.
30. **Papelier Y, Escourrou P, Gauthier JP, and Rowell LB.** Carotid baroreflex control of blood pressure and heart rate in men during dynamic exercise. *J Appl Physiol* 77: 502–506, 1994.

31. **Potts JT and Li J.** Interaction between carotid baroreflex and exercise pressor reflex depends on baroreceptor afferent input. *Am J Physiol Heart Circ Physiol* 274: H1841–H1847, 1998.
32. **Potts JT and Mitchell JH.** Rapid resetting of carotid baroreceptor reflex by afferent input from skeletal muscle receptors. *Am J Physiol Heart Circ Physiol* 275: H2000–H2008, 1998.
33. **Potts JT, Paton JF, Mitchell JH, Garry MG, Kline G, Anguelov PT, and Lee SM.** Contraction-sensitive skeletal muscle afferents inhibit arterial baroreceptor signalling in the nucleus of the solitary tract: role of intrinsic GABA interneurons. *Neuroscience* 119: 201–214, 2003.
34. **Potts JT, Shi XR, and Raven PB.** Carotid baroreflex responsiveness during dynamic exercise in humans. *Am J Physiol Heart Circ Physiol* 265: H1928–H1938, 1993.
35. **Rowell LB and O'Leary DS.** Reflex control of the circulation during exercise: chemoreflexes and mechanoreflexes. *J Appl Physiol* 69: 407–418, 1990.
36. **Rowell LB, O'Leary DS, and Kellogg DS.** Integration of cardiovascular control system in dynamic exercise. In: *Handbook of Physiology. Exercise: Regulation and Integration of Multiple Systems.* Bethesda, MD: Am. Physiol. Soc., sect. 12, pt. II, chapt. 17, 1996, p. 770–838.
37. **Ruble SB, Valic Z, Buckwalter JB, and Clifford PS.** Dynamic exercise attenuates sympathetic responsiveness of canine vascular smooth muscle. *J Appl Physiol* 89: 2294–2299, 2000.
38. **Sato T, Kawada T, Inagaki M, Shishido T, Takaki H, Sugimachi M, and Sunagawa K.** New analytic framework for understanding sympathetic baroreflex control of arterial pressure. *Am J Physiol Heart Circ Physiol* 276: H2251–H2261, 1999.
39. **Stebbins CL, Brown B, Levin D, and Longhurst JC.** Reflex effect of skeletal muscle mechanoreceptor stimulation on the cardiovascular system. *J Appl Physiol* 65: 1539–1547, 1988.
40. **Sun MK and Guyenet PG.** GABA-mediated baroreceptor inhibition of reticulospinal neurons. *Am J Physiol Regul Integr Comp Physiol* 249: R672–R680, 1985.
41. **Victor RG, Rotto DM, Pryor SL, and Kaufman MP.** Stimulation of renal sympathetic activity by static contraction: evidence for mechanoreceptor-induced reflexes from skeletal muscle. *Circ Res* 64: 592–599, 1989.
42. **Waldrop TG, Eldridge FL, Iwamoto GA, and Mitchell JH.** Central neural control of respiration and circulation during exercise. In: *Handbook of Physiology. Exercise: Regulation and Integration of Multiple Systems. Control of Respiratory and Cardiovascular Systems.* Bethesda, MD: Am. Physiol. Soc., 1996, sect. 12, pt. II, chapt. 9, p. 333–380.

Acetylcholine From Vagal Stimulation Protects Cardiomyocytes Against Ischemia and Hypoxia Involving Additive Nonhypoxic Induction of HIF-1α

Yoshihiko Kakinuma, Motonori Ando, *Masanori Kuwabara, Rajesh G. Katare, #Koji Okudela, +Masanobu Kobayashi, Takayuki Sato

Department of Cardiovascular Control, *Department of Medicine and Geriatrics, Kochi Medical School, Nankoku, Japan.
#Department of Pathology, Division of Cellular Pathobiology, Yokohama City University Graduate School of Medicine, Yokohama, Japan.
+Division of Cancer Pathobiology, Institute for Genetic Medicine, Hokkaido University, Sapporo, Japan

Correspondence:Yoshihiko Kakinuma, M.D., Ph.D. Department of Cardiovascular Control Kochi Medical SchoolNankoku, 783-8505, Japan
FAX: +81-88-880-2310 TEL:+81-88-880-2587 E-mail:kakinuma@med.kochi-u.ac.jp

ABSTRACT

Electrical stimulation of the vagal efferent nerve improves the survival of myocardial infarcted rats. However, the mechanism for this beneficial effect is unclear. We investigated the effect of acetylcholine (ACh) on HIF-1α using rat cardiomyocytes under normoxia and hypoxia. ACh posttranslationally regulated HIF-1α and increased its protein level under normoxia. ACh increased Akt phosphorylation, and wortmannin or atropine blocked this effect. Hypoxia-induced caspase-3 activation and mitochondrial membrane potential collapse were prevented by ACh. Dominant-negative HIF-1α inhibited the cell protective effect of ACh. In acute myocardial ischemia, vagal nerve stimulation increased HIF-1α expression and reduced the infarct size. These results suggest that ACh and vagal stimulation protect cardiomyocytes through the PI3K/Akt/HIF-1α pathway.

Key words: acetylcholine, ischemia, apoptosis, protein kinases

1. Introduction

The prognosis of patients with chronic heart failure remains poor, due to progressive remodeling of the heart and lethal arrhythmia. Acute ischemia or hypoxia causes loss of cardiomyocytes, followed by remodeling in the chronic phase. Although various therapeutic approaches have been introduced, including implantable defibrillators [1], a more effective modality of therapy has been anticipated for several years. A recent animal study by Li et al. demonstrated that vagal nerve stimulation prevented ventricular remodeling after myocardial infarction, suggesting a novel therapeutic strategy against heart failure [2]. Furthermore, Krieg et al. reported that acetylcholine (ACh) has a cardioprotective effect [3]. Although nitric oxide (NO) is supposed to be a major signaling molecule induced by ACh, a mechanism for the beneficial effect of vagal nerve stimulation on cardiomyocytes remains to be clarified. To investigate this mechanism, we hypothesized that vagal stimulation or ACh directly triggers a cell survival signal that is subsequently amplified and leads to protection of the cardiomyocytes from acute ischemic conditions, and that this effect of ACh, if continued, could be responsible for chronic cardioprotection.

In the present study, we focused on demonstrating the cellular action of ACh through hypoxia-inducible factor (HIF)-1α. HIF-1α is a transcription factor that is important for cell survival under hypoxia. HIF-1α activates the expression of many genes indispensable for cell survival [4,5]. Under normoxia, the HIF-1α protein level is very low, due to proteasomal degradation through with von Hippel-Lindau tumor suppressor protein (VHL). However, HIF-1α escapes from this degradation under hypoxia, and this is recognized as the hypoxic pathway [6,7]. Recently, it was revealed that HIF-1α can be also induced via a nonhypoxic pathway by angiotensin II [8,9]. Taken together, it is conceivable that HIF-1α induction is one of the adaptation processes to hypoxia and ischemia, and that additional induction of HIF-1α during ischemia via a nonhypoxic pathway could provide further cardioprotection.

Therefore, we investigated the direct effects of ACh on survival signaling in cardiomyocytes and of vagal stimulation on hearts. The results suggest that ACh and vagal stimulation protect cardiomyocytes from acute hypoxia and ischemia via additional HIF-1α protein induction through a nonhypoxic pathway.

2. Materials and Methods

2.1. Cell Culture

To examine the effect of ACh on cardiomyocytes, H9c2 cells as well as primary cardiomyocytes isolated from neonatal rats were used. H9c2 cells, which are frequently used to investigate signal

transduction and channels in rat cardiomyocytes, are derived from rat embryonic ventricular cardiomyocytes. H9c2 cells were incubated in DMEM containing 10% FBS and antibiotics. Primary cardiomyocytes were isolated from 2-3-day-old neonatal WKY rats and incubated in DMEM/Ham F-12 containing 10% FBS. HEK293 cells and HeLa cells cultured in DMEM containing 10% FBS were also used.

2.2. Western Blot Analysis

H9c2 cells and primary cardiomyocytes were treated with 1 mM ACh to evaluate expression of HIF-1a protein under normoxia or with 1 mM S-nitroso-N-acetylpenicillamine (SNAP) to study the signal transduction. To investigate the signal transduction, H9c2 cells were pretreated with a PI3K inhibitor, (wortmannin; 300 nM), a muscarinic receptor, (atropine; 1 mM), a transcriptional inhibitor, (actinomycin D; 0.5 μg/ml) or a protein synthesis inhibitor, (cycloheximide; 10 μg/ml), followed by ACh treatment. Cell lysates were mixed with a sample buffer, fractionated by 10% SDS-PAGE and transferred onto membranes. The membranes were incubated with primary antibodies against HIF-1a (Santa Cruz Biotechnology, Santa Cruz, California, USA), Akt and phospho-Akt (Cell Signaling Technology, Beverly, Massachusetts, USA), and α-tubulin (Lab Vision, Fremont, California, USA), and then reacted with an HRP-conjugated secondary antibody (BD Transduction Laboratories, San Diego, California, USA). Positive signals were detected with an enhanced chemiluminescence system (Amersham, Piscataway, New Jersey, USA). In each study, the experiments were performed in duplicate and repeated 3-5 times (n=3-5). Representative data are shown.

2.3. MTT Activity Assay

To evaluate the effects of hypoxia and ACh on the mitochondrial function of cardiomyocytes, we measured 3-(4,5-dimethylthiazol-2-yl)-2,5-diphenyl tetrazolium bromide (MTT) reduction activity in H9c2 or HEK293 cells under hypoxia (1% oxygen concentration), in the presence or absence of ACh. The cells were pretreated with 1 mM ACh for 12 hours, and then subjected to hypoxia for 12 hours. At 4 hours before sampling, the MTT reagents were added to the culture and incubated.

2.4. Caspase-3 Activity Assay

Caspase-3 activity was measured using a CPP32/Caspase-3 Fluorometric Protease Assay Kit, (CHEMICON INTERNATIONAL, Temecula, California, USA). Hypoxia-treated H9c2 cells with or without 1 mM ACh pretreatment were lysed and the cytosolic extract was added to the caspase-3 substrate. A fluorometer equipped with a 400-nm excitation filter and 505-nm emission filter was used to measure the samples.

2.5. DePsipher Assay

To examine the effects of hypoxia and ACh on the mitochondrial electrochemical gradient, we analyzed cardiomyocytes using a DePsipher™ Mitochondrial Potential Assay Kit (Trevigen, Gaithersburg, Maryland, USA). Apoptotic cells, which undergo mitochondrial membrane potential collapse cannot accumulate the DePsipher reagent in their mitochondria. As a result, apoptotic cells show decreased red fluorescence in their mitochondria, and the reagent remains in the cytoplasm as a green fluorescent monomer. Therefore, apoptotic cells were easily differentiated from healthy cells, which showed more red fluorescence.

2.6. Evaluation of NO production

NO production was measured using the 4,5 diaminofluoresceindiacetate (DAF-2DA; Alexis, Lausen, Switzerland) fluorometric NO detection system as previously reported [10]. The intensity of the DAF-2DA green fluorescence in ACh-treated cells was measured and compared with that in non-treated cells (λ Ex. 492 nm; λ Em. 515 nm).

2.7. Transfection

To investigate the direct contribution of Akt phosphorylation to HIF-1a stabilization or that of HIF-1a to the ACh effect, HEK293 cells were transfected with an expression vector for wild-type Akt (wt Akt), dominant-negative Akt (dn Akt), wild-type HIF-1α (wt HIF-1α) or dominant-negative HIF-1α (dn HIF-1α), using Effectene (Qiagen, Valencia, California, USA) according to the manufacture's protocol. The Akt vectors were generous gifts from by Dr. K. Okudela (Yokohama City University, Kanagawa, Japan) [11], while the HIF-1α vectors were kindly provided by Dr. M. Kobayashi (Hokkaido University, Sapporo, Japan) [12]. After transfection, HEK293 cells were pretreated with 1 mM ACh for 12 hours, followed by evaluating the HIF-1α protein level or by hypoxia for 12 hours and MTT activity in each group was evaluated. As a control, cells were transfected with a vector for green fluorescent protein (GFP).

2.8. RT-PCR

Total RNA was isolated from H9c2 cells according to a modified acid guanidinium-phenol-chloroform method using an RNA isolation kit (ISOGEN; Nippon Gene, Tokyo, Japan), and reverse-transcribed to obtain a first-strand cDNA. This first-strand cDNA was amplified by specific primers for HIF-1a, and the PCR products were fractionated by electrophoresis.

2.9. Vagal Nerve Stimulation in Myocardial Ischemia

Left ventricular myocardial ischemia (MI) was performed by 3 hours of left coronary artery (LCA) ligation in anesthetized 9-week-old male Wistar rats

under artificial ventilation previously described [3]. Sham-operated (control) rats did not undergo LCA ligation. For vagal nerve stimulation (VS), the right vagal nerve in the neck was isolated and cut. Only the distal end of the vagal nerve was stimulated in order to exclude the effects of the vagal afferent. The electrode was connected to an isolated constant voltage stimulator. VS was performed from 1 min before the LCA ligation until 3 hours afterwards, using 0.1 ms pulses at 10 Hz (MI-VS). The electrical voltage of the pulses was adjusted to obtain a 10% reduction in the heart rate before LCA ligation, but VS (MI-VS) was not associated with any blood pressure reduction during the experiments, compared with MI. At the end of the experiments, the rats were either injected with 2 ml of 2% Evans blue dye via the femoral vein to measure the risk area followed by determination of the infarct size with 2% triphenyl tetrazolium chloride (TTC) staining or the heart was excised for protein isolation and subsequent western blotting to detect HIF-1a protein. The percentage of the infarcted area of the left ventricle (LV) was calculated as the ratio of the infarcted area to the risk area.

2.10. Densitometry

The western blotting data were analyzed using Kodak 1D Image Analysis Software (Eastman Kodak Co., Rochester, New York, USA).

2.11. Statistics

The data were presented as means ± S.E. The mean values between two groups were compared by the unpaired Student's t test. Differences among data were assessed by ANOVA for multiple comparisons of results. Differences were considered significant at $P<0.05$.

3. Results

3.1. Posttranslational Regulation of HIF-1α by ACh through a Nonhypoxic Pathway

ACh (1 mM) increased HIF-1α protein expression in H9c2 cells under normoxia (Fig. 1A). ACh increased NO production, as evaluated by DAF-2DA (Figure 1B), suggesting that NO is involved in the signal transduction of HIF-1a induction. Actinomycin D (0.5 μg/ml; Figs. 2A, 2B) and cycloheximide (10 μg/ml; Fig. 2C) did not decrease the HIF-1α level under normoxia, suggesting that HIF-1α degradation is regulated by ACh. Furthermore, ACh increased HIF-1 α level in primary cardiomyocytes without reducing their beating rate (Fig. 3). Since H9c2 cells did not beat, these results suggest that HIF-1α induction is independent of the heart rate-decreasing effect of ACh.

3.2. Akt Phosphorylation by ACh

ACh had no effect on the total Akt protein level, but increased Akt phosphorylation (Fig. 4A) as effectively as SNAP (data not shown). The ACh-induced Akt phosphorylation was inhibited by atropine in a dose-dependent manner (Fig. 4B). ACh-induced Akt phosphorylation and its inhibition by atropine were also observed in rat primary cardiomyocytes (Fig. 4C).

3.3. PI3K/Akt Pathway for HIF-1α induction by ACh

Wortmannin completely inhibited the ACh-induced Akt phosphorylation (Fig. 4D), in clear contrast to the data in Fig. 4A. Furthermore, it also attenuated the HIF-1α induction by ACh (Fig. 4E). To elucidate the contribution of Akt phosphorylation to HIF-1α protein level in normoxia, dn Akt was introduced into HEK293 cells, and found to partially inhibit the HIF-1α induction by ACh (Fig. 4F).

3.4. Effect of ACh on Apoptosis during Hypoxia

The DePsipher assay clearly showed that hypoxia (1% oxygen concentration) for 12 hours caused mitochondrial membrane potential collapse leading to cell death, and that 1 mM ACh inhibited this collapse in H9c2 cells (Fig. 5A). ACh attenuated the decrease in MTT activity caused by 12 hours of hypoxia in H9c2 cells (Fig. 5B; 103.4±0.8% in ACh+hypoxia vs. 56.6±0.7% in hypoxia, $p<0.01$, n=8) and HEK293 cells ($p<0.01$ vs. hypoxia). The caspase-3 activity was increased by hypoxia in H9c2 cells, and pretreatment with 1 mM ACh inhibited this increase (Fig. 5C; 128±2% in hypoxia vs. 90±2% in ACh+hypoxia, $p<0.01$, n=4). To elucidate the dependency of the ACh-induced protective effect on HIF-1α, dn HIF-1α was transfected into HEK293 cells, followed by ACh pretreatment and then hypoxia. It was found that dn HIF-1α inhibited the protective effect of ACh from hypoxia (Fig. 5D; 115.1±1.2% in wt HIF-1α and 111.8±1.8% in GFP vs. 59.0±3.4% in dn HIF-1α, $p<0.05$, n=10), suggesting that HIF-1α induction by ACh is partially responsible for the protective effect.

3.5. Effect of Vagal Stimulation on HIF-1a in Myocardial Ischemia

To evaluate the significance of ACh for cardioprotection in vivo, the vagal nerve was stimulated prior to the myocardial ischemia. Histological analysis demonstrated a tendency for the infarcted area from the vagal nerve-stimulated (MI-VS) hearts to be smaller than that from non-stimulated (MI) hearts (31.5±4.6% in MI-VS vs. 40.9±2.5% in MI, n=3), even though the risk areas (non-perfused areas) were comparable (Fig. 6A; 59.2±1.0% in MI-VS vs. 53.7±1.0% in MI, n=3). In the MI-VS hearts, the HIF-1α protein level was further elevated compared to that in the MI hearts (Fig. 6B; 244±24% in MI-VS vs. 112±1% in MI, n=3). These results suggest that vagal nerve stimulation in the ischemic heart activates both the hypoxic and nonhypoxic pathways of HIF-1α

induction, resulting in increased induction of HIF-1a.

3.6. Nonhypoxic Induction of HIF-1α in Other Cells

The observed ACh-mediated HIF-1α induction was not limited to H9c2 or primary cultured cardiomyocytes, but also found in several other types of cell lines, including HEK293, and HeLa cells (Figure 7). Since these cells did not beat spontaneously, the results suggest that the system of ACh-mediated HIF-1α induction is not only independent of the beating rate of cardiomyocytes, but also a generally conserved system in cells.

4. Discussion

Cardioprotective Action by ACh and Vagal Stimulation via the Muscarinic Receptor

Using animal models, several studies have shown that accentuated antagonism against the sympathetic nervous system is a major mechanism for the beneficial effect of vagal tone on the ischemic heart [13]. Although ACh was involved in triggering preconditioning mechanisms in an ischemia-reperfusion model [3], it remained unclear whether vagal nerve stimulation in acute ischemia or hypoxia followed these mechanisms. In the present study, we have disclosed that ACh possesses a protective effect on cardiomyocytes. In rat cardiomyocytes, ACh triggered a sequence of survival signals through Akt that eventually induced HIF-1α, inhibited the collapse of the mitochondrial membrane potential and decreased caspase-3 activity, thereby leading to the survival of cardiomyocytes under hypoxia. Furthermore, our results suggest ACh exerts this action through Akt in other cells. The current study therefore provides another insight into the cellular mechanism for the cardioprotective effects of ACh and vagal stimulation.

Signaling Pathway of ACh via PI3K/Akt and Antiapoptotic Effects of ACh

Since previous studies demonstrated that a PI3K inhibitor greatly reduced HIF-1α induction in heart and renal cells [14,15] and a few studies have reported that MAP kinase is activated through ACh, we focused on the PI3K/Akt pathway, one of the important cell survival signaling pathways [16], and found that ACh directly activated Akt phosphorylation via PI3K. PI3K/Akt signaling has been reported to have an antiapoptotic activity through various features, such as inhibition of Bad-binding to Bcl-2, caspase 9, Fas and glycogen synthetase kinase-3 [17,18]. These facts imply a definite involvement of Akt activation in cell survival. As shown using dn HIF-1α, ACh inhibited hypoxia-induced cell death through HIF-1α induction via Akt phosphorylation. These results indicate that ACh actually protects cardiomyocytes from hypoxia at the cellular level.

Additional Induction of HIF-1α by ACh and Vagal Stimulation

HIF-1α regulates the transcriptional activities of very diverse genes involved in cell survival and is itself regulated at the posttranslational level by VHL [4,6,7]. Recent studies have shown that HIF-1α is also regulated through a nonhypoxic pathway involving angiotensin II, TNF-α and NO [8,9,19,20]. Therefore, it is speculated that cardiomyocytes possess a similar system for regulating HIF-1α through ACh, independent of the oxygen concentration. Induction of HIF-1α is a powerful cellular response against hypoxia, and further increases in its expression by other pathways may be beneficial. The present results indicate that the significance of ACh or vagal nerve stimulation in hypoxic stress can be attributed to additional HIF-1α induction through dual induction pathways, i.e., hypoxic and nonhypoxic pathways.

The present study has revealed that ACh-mediated HIF-1α induction is widely conserved in other cells. Consistent with a previous report [10], the current results suggest that NO is produced by ACh. According to a report that NO attenuates the interaction between pVHL and HIF-1α through inhibiting PHD activity [21], it is possible that ACh may increase the HIF-1α protein level through NO. Recent studies conducted by Krieg et al. and Xi et al., have provided supportive data compatible with our results [3,22], while another study by Hirota et al. also revealed a nonhypoxic pathway for HIF-1α induction by ACh in a human kidney-derived cell line [23].

The signaling pathway of the muscarinic receptor has been studied extensively, and many pathways are involved in its specific biological effects. Therefore, possible involvement of other pathways in the nonhypoxic induction of HIF-1α cannot be excluded. However, it was demonstrated that dn Akt and dn HIF-1α decreased the effect of ACh. Consistent with a recent study [24], we have revealed that ACh or vagal stimulation protects cardiomyocytes in the acute phase. This observation suggests that the protective effect in the acute phase may result in inhibition of cardiac remodeling in the chronic phase, since vagal stimulation produces additional HIF-1α induction through a nonhypoxic pathway, which increases cell survival.

Acknowledgement

This study was supported by a Health and Labor Sciences Research Grant (H15-PHYSI-001) for Advanced Medical Technology from the Ministry of Health, Labor, and Welfare of Japan.

References

1. Julian D.G, Camm A.J., Frangin G, Janse M.J., Munoz A., Schwartz P.J., Simon P. (1997) Randomised trial of effect of amiodarone on mortality

in patients with left-ventricular dysfunction after recent myocardial infarction: EMIAT. European Myocardial Infarct Amiodarone Trial Investigators. *Lancet* 349, 667-674.
2. Li M., Zheng C., Sato T., Kawada T., Sugimachi M., Sunagawa K. (2004) Vagal nerve stimulation markedly improves long-term survival after chronic heart failure in rats. *Circulation* 109, 120-124.
3. Krieg T., Qin Q., Philipp S., Alexeyev M.F., Cohen M.V., Downey J.M. (2004) Acetylcholine and bradykinin trigger preconditioning in the heart through pathway that includes Akt and NOS. *Am. J. Physiol. Heart Circ. Physiol.* 287, H2606-H2611.
4. Semenza G.L. (2003) HIF-1, O(2), and the 3 PHDs: how animal cells signal hypoxia to the nucleus. *Cell* 107, 1-3.
5. Kakinuma Y., Miyauchi T., Yuki K., Murakoshi N., Goto K., Yamaguchi I. (2001) Novel molecular mechanism of increased myocardial endothelin-1 expression in the failing heart involving the transcriptional factor hypoxia-inducible factor-1a induced for impaired myocardial energy metabolism. *Circulation* 103, 2387–2394.
6. Maxwell P.H., Wiesener M.S., Chang G.W., Clifford S.C., Vaux E.C., Cockman M.E., Wykoff C.C., Pugh C.W., Maher E.R., Ratcliffe P.J. (1999) The tumour suppressor protein VHL targets hypoxia-inducible factors for oxygen-dependent proteolysis. *Nature* 399, 271-275.
7. Min J.H., Yang H., Ivan M., Gertler F., Kaelin W.G. Jr., Pavletich N.P. (2002) Structure of an HIF-1alpha -pVHL complex: hydroxyproline recognition in signaling. *Science* 296, 1886-1889.
8. Page E.L., Robitaille G.A., Pouyssegur J., Richard D.E. (2002) Induction of hypoxia-inducible factor-1alpha by transcriptional and translational mechanisms. *J. Biol. Chem.* 277, 48403-48409.
9. Richard D.E., Berra E., Pouyssegur J. (2000) Nonhypoxic pathway mediates the induction of hypoxia-inducible factor 1alpha in vascular smooth muscle cells. *J. Biol. Chem.* 275, 26765-26771.
10. Zanella B., Calonghi N., Pagnotta E., Masotti L., Guarnieri C. (2002) Mitochondrial nitric oxide localization in H9c2 cells revealed by confocal microscopy. *Biochem. Biophys. Res. Commun.* 290, 1010-1014.
11. Okudela K., Hayashi H., Ito T., Yazawa T., Suzuki T., Nakane Y., Sato H., Ishi H., KeQin X., Masuda A., Takahashi T., Kitamura H. (2004) K-ras gene mutation enhances motility of immortalized airway cells and lung adenocarcinoma cells via Akt activation: possible contribution to non-invasive expansion of lung adenocarcinoma. *Am. J. Pathol.* 164, 91-100.
12. Chen J., Zhao S., Nakada K., Kuge Y., Tamaki N., Okada F., Wang J., Shindo M., Higashino F., Takeda K., Asaka M., Katoh H., Sugiyama T., Hosokawa M., Kobayashi M. (2004) Dominant-negative hypoxia-inducible factor-1 alpha reduces tumorigenicity of pancreatic cancer cells through the suppression of glucose metabolism. *Am. J. Pathol.* 162, 1283-1291.
13. Du X.J., Dart A.M., Riemersma R.A., Oliver M.F. (1990) Failure of the cholinergic modulation of norepinephrine release during acute myocardial ischemia in the rat. *Circ. Res.* 66, 950-956.
14. Kim C.H., Cho Y.S., Chun Y.S., Park J.W., Kim M.S. (2002) Early expression of myocardial HIF-1alpha in response to mechanical stresses: regulation by stretch-activated channels and the phosphatidylinositol 3-kinase signaling pathway. *Circ. Res.* 90, e25-e33.
15. Sandau K.B., Zhou J., Kietzmann T., Brune B. (2001) Regulation of the hypoxia-inducible factor 1alpha by the inflammatory mediators nitric oxide and tumor necrosis factor-alpha in contrast to desferroxamine and phenylarsine oxide. *J. Biol. Chem.* 276, 39805-39811.
16. Vanhaesebroeck B., Alessi D.R. (1999) The regulation and activities of the multifunctional serine/threonine kinase Akt/PKB. *Exp. Cell Res.* 253, 210-229.
17. Kennedy S.G., Wagner A.J., Conzen S.D., Jordan J., Bellacosa A., Tsichlis P.N., Hay N. (1997) The PI3-kinase/Akt signaling pathway delivers an anti-apoptotic signal. *Genes Dev.* 11, 701-713.
18. Cross D.A., Alessi D.R., Cohen P., Andjelkovich M., Hemmings B.A. (1995) Inhibition of glycogen synthase kinase-3 by insulin mediated by protein kinase B. *Nature* 378, 785-789.
19. Zhou J., Schmid T., Brune B. (2003) Tumor necrosis factor-alpha causes accumulation of a ubiquitinated form of hypoxia inducible factor-1alpha through a nuclear factor-kappaB-dependent pathway. *Mol. Biol. Cell* 14, 2216-2225.
20. Sandau K.B., Fandrey J., Brune B. (2001) Accumulation of HIF-1alpha under the influence of nitric oxide. *Blood* 97, 1009-1015.
21. Metzen E., Zhou J., Jelkmann W., Fandrey J., Brune B. (2003) Nitric oxide impairs normoxic degradation of HIF-1alpha by inhibition of prolyl hydroxylases. *Mol. Biol. Cell* 14, 3470-3481.
22. Xi L., Taher M., Yin C., Salloum F., Kukreja R.C. (2004) Cobalt chloride induces delayed cardiac preconditioning in mice through selective activation of HIF-1{alpha} / AP-1 and iNOS Signaling. *Am. J. Physiol. Heart. Circ. Physiol.* 287, H2369-H2375.
23. Hirota K., Fukuda R., Takabuchi S., Kizaka-Kondoh S., Adachi T., Fukuda K., Semenza G.L. (2004) Induction of hypoxia-inducible factor 1 activity by muscarinic acetylcholine receptor signaling. *J. Biol. Chem.* 279, 41521-41528.
24. Wang H., Yu M., Ochani M., Amella C.A., Tanovic M., Susarla S., Li J.H., Wang H., Yang H., Ulloa L., Al-Abed Y., Czura C.J., Tracey K.J. (2003) Nicotinic acetylcholine receptor alpha7 subunit is an essential regulator of inflammation. *Nature* 421, 384-388.

Figure legends

Figure 1

HIF-1a is induced by ACh in rat cardiomyocytes even under normoxia.

A. After treatment of H9c2 cells with 1 mM ACh for 8 hours, the HIF-1a protein level is increased (# $p<0.05$ vs. control, n=4). **B.** ACh (1 mM) increases the intensity of DAF-2DA fluorescence (# $p<0.01$ vs. control, n=3).

Figure 2

HIF-1α induction by ACh is posttranslationally regulated in rat cardiomyocytes under normoxia.

A. The HIF-1α protein level in H9c2 cells in the presence of 0.5 μg/ml of actinomycin D is increased by 1 mM ACh to a comparable level to

that in the absence of actinomycin D (N.S., not significant, n=3). **B.** Actinomycin D does not decrease the HIF-1α mRNA level, as evaluated by RT-PCR. **C.** Cycloheximide (10 μg/ml) does not affect the HIF-1α protein level (n=3).

Figure 3
Rat primary cultured cardiomyocytes show comparable HIF-1α induction by 1 mM ACh to that in H9c2 cells (# $p<0.05$ vs. control, n=3).

Figure 4
Akt is activated by ACh in rat cardiomyocytes, leading to HIF-1α induction.
A. Akt phosphorylation in H9c2 cells is rapidly increased by 1 mM ACh (# $p<0.05$ vs. baseline, n=4), whereas the total protein level of Akt remains unaffected. **B.** The ACh-induced increase in Akt phosphorylation is blocked by 1 mM atropine (# $p<0.05$ vs. 0 μM atropine, n=3). **C.** ACh (1 mM) also increases Akt phosphorylation in rat primary cardiomyocytes (# $p<0.05$ vs. baseline, n=3), and atropine blocks this effect. **D.** Pretreatment with 300 nM wortmannin completely inhibits ACh-induced Akt phosphorylation in H9c2 cells (N.S., not significant, n=3). **E.** Wortmannin (300 nM) also inhibits HIF-1α induction by ACh (# $p<0.05$ vs. wortmannin (+), n=3). Each figure shows a representative result from 3 independently performed experiments (n=3). **F.** In contrast to wt Akt, HIF-1α induction y ACh is blocked by dn Akt in HEK293 cells (n=4).

Figure 5
Collapse of the mitochondrial membrane potential in rat cardiomyocytes under hypoxia is attenuated by ACh pretreatment.
A. Hypoxia decreases the mitochondrial membrane potential in H9c2 cells within 12 hours. Red spots are decreased by hypoxia, whereas pretreatment with 1 mM ACh for 12 hours inhibits this effect. **B.** Pretreatment with 1 mM ACh inhibits the decrease in MTT reduction activity induced by 12 hours of hypoxia not only in H9c2 cells (# $p<0.01$ vs. hypoxia, n=8) but also in HEK293 cells (* $p<0.01$ vs. hypoxia, n=8). **C.** Hypoxia increases caspase-3 activity, whereas pretreatment with 1 mM ACh inhibits this effect (# $p<0.01$ vs. hypoxia, n=3). **D.** In contrast to wt HIF-1α or GFP, dn HIF-1α alone decreases the MTT activity under hypoxia after ACh treatment (# $p<0.01$ vs. wt and GFP, * $p<0.05$ vs. non-transfection, n=10).

Figure 6
Vagal nerve stimulation decreases infarcted area with increased HIF-1a expression.
A. A quantitative analysis reveals comparable non-perfused areas in both vagal-stimulated (MI-VS) and non-stimulated (MI) hearts, whereas the infarcted area identified by TTC staining is smaller in the MI-VS heart than in the MI heart. **B.** HIF-1α induction in the ischemic heart is increased by vagal stimulation (MI-VS) compared with that in ischemia alone (MI) (#, $p<0.01$ vs. MI) (n=3).

Figure 7
HIF-1a is induced by ACh under normoxia in other cells.
ACh (1 mM) increases HIF-1a protein level in HEK293 and HeLa cells (n=3 each) under normoxia.

Kakinuma Y et al
Figure 1

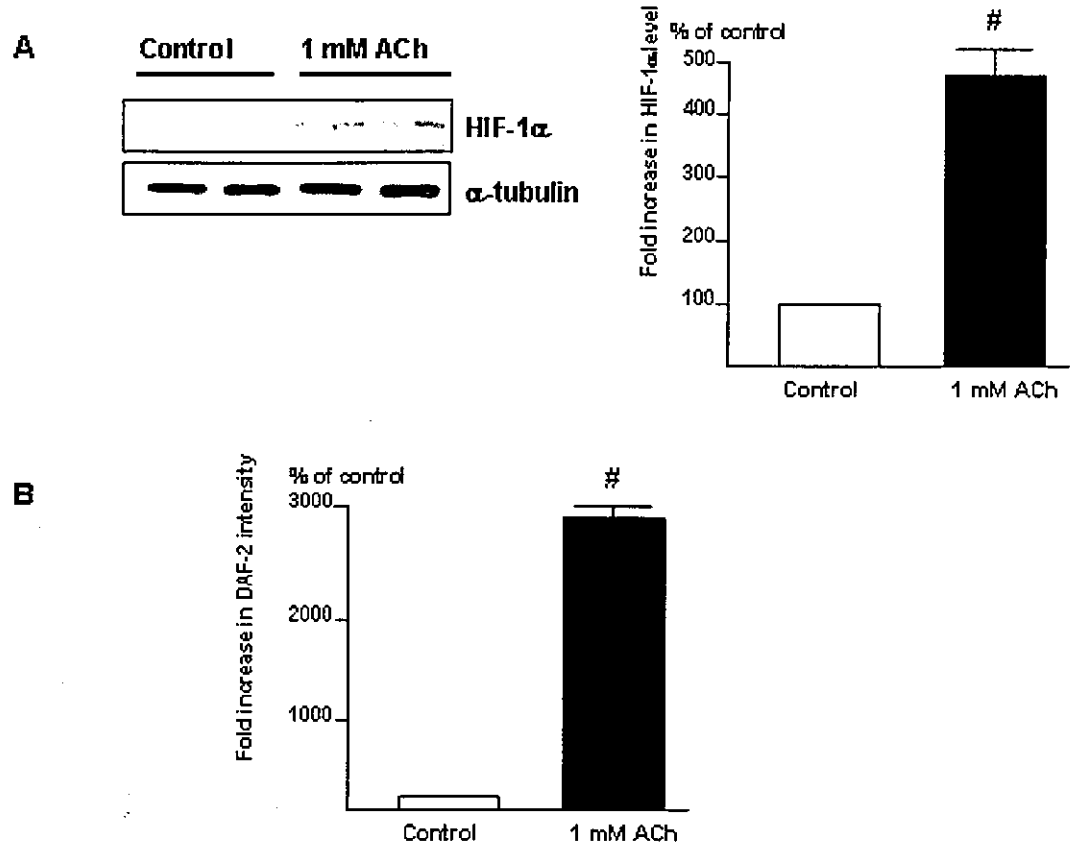

Figure 2

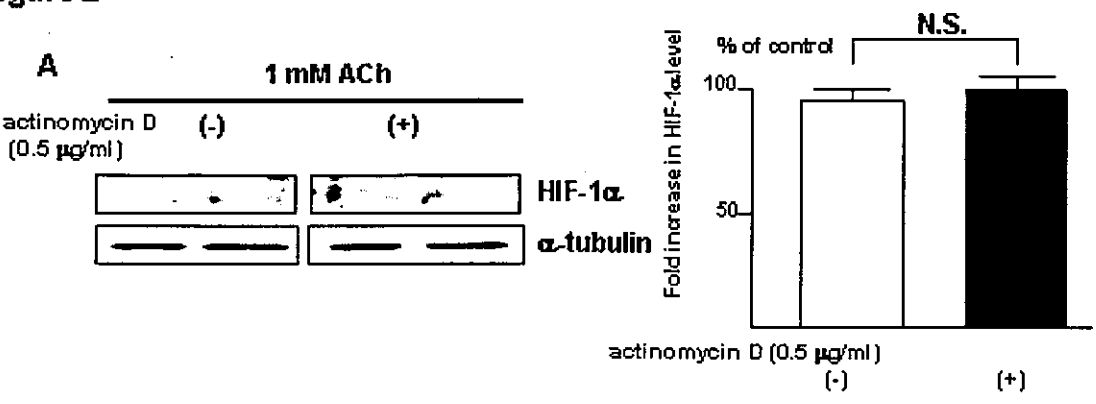

Kakinuma Y et al
Figure 2

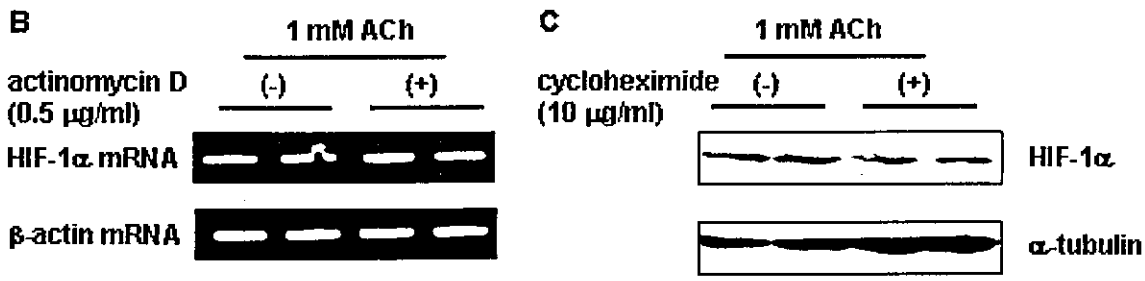

Figure 3

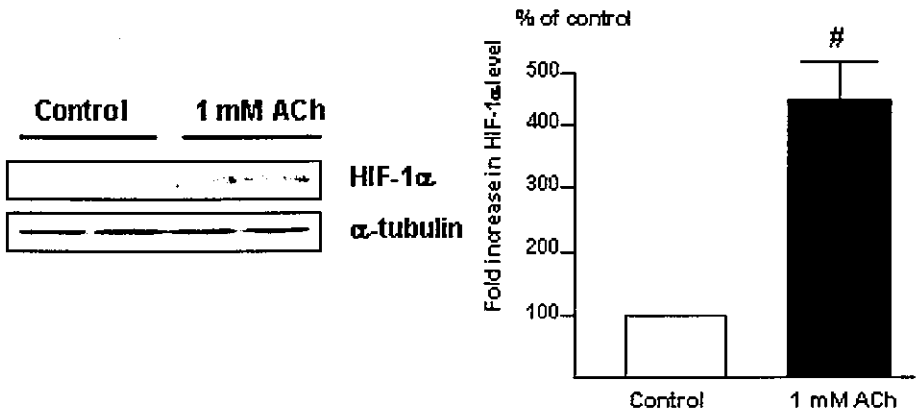

Figure 4

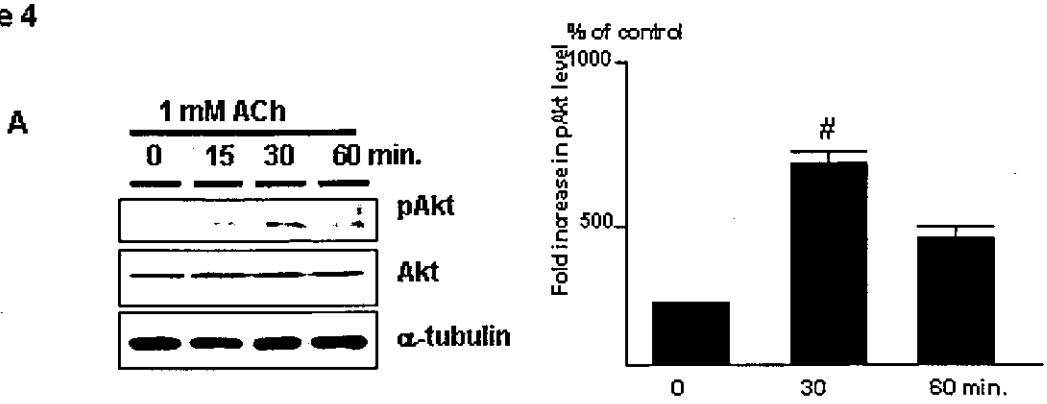

Kakinuma Y et al
Figure 4